EXCITONIC EFFECTS IN MAGNESIUM OXIDE: *AB INITIO* STUDY

Master Thesis

Tetiana Khotiaintseva

Supervisor: Francesco Sottile, PhD
Theoretical Spectroscopy group,
Laboratoire des Solides Irradiés,
École Polytechnique, France

June 2015

Acknowledgements

I would like to thank my supervisor Francesco Sottile for opening the wonderful world of theoretical spectroscopy for me. I am very greatful for his optimism and patience, for support, guidance and always having time to help; without him, this thesis would not be possible.

I would also like to thank Lucia Reining for her advice, wisdom and openness. I am honored to have met a great physicist and a great leader like her. I thank Lucia for showing me what science is all about, and for teaching me the value of collaboration and networking in research.

I also thank Matteo Gatti for organising the discussion group, which helped me greatly to understand solid state physics, and for always being open to discussions.

I am grateful to all members of the Theoretical Spectroscopy group in Palaiseau for their friendship, support and fruitful discussions, in particular to Marco Vanzini for teaching me Feynman's diagrams, to Igor Reshtnyak for introducing me to the group, and to organizing comittee of Young Researchers Meeting of European Theoretical Spectroscopy Facility for awesome conference and for letting me be a part of the organization process.

I am deeply idebted to my university professor Oleksiy Kolezhuk, who introduced me to quantum mechanics, and taught me a lot of wonderful things; he made me believe in myself, and without him I would never dare to make this step in the field of electronic structure calculations.

I acknowledge my gratitude to Lifelong Learning Programme of European Comission and to the SEPRP-Chem master programme for giving me the opportunity to study abroad, and to Sandrine Lacombe who organised this master programme and made it successful. I also thank to all the SERP-Chem students who stood beside me during the master studies, and who became my dearest friends. Lipsa Nag, Cathy Wu, and Mikalil Lo, I am so grateful for the time we spent together, you made these two years unforgettable.

Finally, I am eternally grateful to my husband Alan Andrzejewski, whose support, encouragement and love made this work much more fruitful and productive.

Contents

Abbreviations

ALDA	adiabatic local-density approximation
BO	Borh-Oppenheimer
BSE	Bethe-Salpeter equation
BZ	Brillouin zone
DFT	density functional theory
e.g.	exempli gratia (“for example”)
GGA	generalized gradient approximation
HF	Hartree-Fock
HK	Hohenberg-Kohn
i.e.	id est (“that is”)
IXS	inelastic X-Ray scattering
KS	Kohn-Sham
LDA	local density approximation
LF	local fields
MBPT	many-body perturbation theory
NIXS	nonresonsnt inelastic X-Ray scattering
RIXS	resonant intelastic X-Ray scattering
RPA	random phase approximation
TDDFT	time-dependent density functional theory
xc	exchange-correlation

Introduction

Excitons are many-body excitations that originate from interaction between an electron, in the otherwise empty conduction band, and a hole, in the otherwise filled valence band, screened by the rest of the electrons. Excitonic effects dominate low-energy part of the optical and loss spectra. Excitons are of paramount importance in many semiconductor applications such as photovoltaics, photocatalysis, light-emitting diodes and so on. It is important to understand the mobility and migrations of excitons, which is related to their energy dispersion as a function of momentum transfer $\mathbf{q}$.

Optical absorption probes the $\mathbf{q} \to 0$ limit, and the most accurate theoretical tool to describe optical spectra is the Bethe-Salpeter equation from the many-body perturbation theory. Modern loss spectroscopies – coherent inelastic X-ray scattering (CIXS), resonant inelastic X-ray scattering (RIXS), Compton scattering – make it possible to study excitons at finite $\mathbf{q}$, and map the full momentum-energy exciton dispersion. Theoretical tools to interpret the experimental results and explore the excitons at large momentum transfer based on bethe-Salpeter equation have only recently been developed [1], allowing us to describe and understand exciton dispersion.

The goal of this work is to apply the newly developed method to a prototypical oxide material, and also to study a material with Wannier-like excitons, which have not been studied yet within *ab initio* theory. The material of choice is Magnesium Oxide, which is a prototype material for insulating oxides, widely used in optoelectronic devices. It is an sp semiconductor with a band gap of 7.8 eV. It has rock salt crystal structure, and belongs to the face centred cubic symmetry group, together with many other important materials. MgO is used as a substrate, and is a part of mixed oxide materials, such as ZnMgO and $MgAl_2O_4$.

This work is divided into three chapters. In the first, we describe briefly the *ab initio* methods that we used for calculations of electronic structure and excited state properties:

- Density functional theory (DFT) for the calculation of ground state density and bands structure;
- Theoretical description of spectroscopic properties;
- Time-dependent density functional theory (TDDFT) for the calculation of optical properties;
- Green's function formalism of the quantum field theory in the many-body physics: GW approximation and the G^0W^0corrections of the band gap energy, Bethe-Salpeter equation (BSE) for the calculation of optical and loss properties and the study of excitons both at $\mathbf{q} \to 0$ limit and finite $\mathbf{q}$.

In the second chapter, we describe the practical implementation of these theoretical approaches in the Abinit and DP/EXC codes that we used for calculations.

And finally in the third chapter we present and discuss the obtained results.

Chapter 1

Theoretical Background

1.1 The many-body problem

The purpose of quantum mechanical calculations is to predict the properties of materials from the first principles, or *ab initio*, such as electronic density, electron addition and removal energies, the response of the system to an external perturbation. All these properties are often encompassed in a polymorphic name "electronic structure". The equation of motion for the electrons of mass m_e with coordinates $\mathbf{r}_i$ and nuclei of mass M_I with coordinates $\mathbf{R}_I$ is the famous non-relativistic Schrödingier equation: $i\hbar\frac{\partial}{\partial t}\Psi = \hat{\mathscr{H}}\Psi$, where $\hat{\mathscr{H}}$ is the many-body Hamiltonian, which in the abscence of external potentials is:

$$\hat{\mathscr{H}} = -\sum_i \frac{\hbar^2\nabla_i^2}{2m_e} - \sum_I \frac{\hbar^2\nabla_i^2}{2M_I} + \frac{1}{2}\sum_{i\neq j}\frac{e^2}{|\mathbf{r}_i - \mathbf{r}_j|} - \sum_{iI}\frac{Z_I e^2}{|\mathbf{r}_i - \mathbf{R}_I|} + \frac{1}{2}\sum_{I\neq J}\frac{Z_I Z_J e^2}{|\mathbf{R}_I - \mathbf{R}_J|}$$

The first two terms are the kinetic terms for electrons and nuclei, and the other three terms is the instanteneous Coulomb interaction between all pairs of bodies. By solving the corresponding eigenvalue problem $\hat{\mathscr{H}}\Psi_n = E_n\Psi_n$ we find the stationary wavefunctions, which depend on all nuclear and electronic variables, and corresponding energies E_n of the system. The wavefunctions contain all information about the system, but even though we can write the Hamiltonian exactly for any system, it cannot be solved analytically for a system which contains more than two bodies, yet alone for a solid with 10^{23} interacting particles. So, inevitably, we have to adopt some approximations to solve the problem, or find a way to extract the information we need without finding the eigenfunctions of the system.

The Born-Oppenheimer approximation allows us to decouple motion of electrons from nuclei. However, solving the Shrödinger equation for electronic problem is still not feasible. All the methods of electronic structure calculation can be separated into two categories:

- wavefunction-based methods
- integrated variable methods

The wavefunction-based methods—for instance, Hartree-Fock, CI, MP2, quantum Monte-Carlo—deal directly with the wavefunctions, trying to find the solutions of the electronic Hamiltonian (often approximated). These methods are mostly used to study molecules, as the number of electrons is relatively small, and computational cost scales quite unfavorably with the numer of electrons.

However, we usually want to know only limited amount of information which is of practial interest to us. The integrated variable methods abandon the idea of following single electrons and instead aim at finding the relevant information about observables bypassing the many-body wavefunctions. The integrated variables are obtained from the full wavefunction by integrating over all but a few variables: for instance, ground state electronic density $n_0(\mathbf{r})$, density matrix $\gamma(\mathbf{r}, \mathbf{r}')$, one-particle Green's function $G(\mathbf{r}, t, \mathbf{r}', t')$ (which can be though of as a dynamical density matrix), and so on.

Each of these basic variables is suitable for evaluation of certain observables: to find the total energy of a system, one can use ground state density, but to find electron removal energies, one has to

use more advanced formalism of Green's functions. It is crucial to know which experiment one wants to describe and choose the cheapest consistent theory.

1.2 Ground state properties and density functional theory

Density functional theory (DFT) is based on the assumption that *any* property of a many-body system can be seen as a functional of its ground state electronic density $n_0(\mathbf{r})$. The existence of such functionals was proven by Hohenberg and Kohn in the landmark paper [2], where they stated the two fundamental theorems of DFT (as presented in [3]):

Theorem I.

"For any system of interacting particles in an external potential $V_{ext}(\mathbf{r})$, the potential $V_{ext}(\mathbf{r})$ is determined uniquely, except for a constant, by the ground state particle density $n_0(\mathbf{r})$."

Theorem II.

"A universal functional of the energy $E[n]$ in terms of the density $n(\mathbf{r})$ can be defined, valid for any external potential $V_{ext}(\mathbf{r})$. For any particular $V_{ext}(\mathbf{r})$, the exact ground state energy of the system is the global minimum value of this functional, and the density that minimises this functional is the exact ground state density $n_0(\mathbf{r})$."

While the Hohenberg-Kohn theorems prove the existence of the funcitonals of the grouns state density, they say nothing about how to find them. What made DFT useful is the Kohn-Sham ansatz, which replaces the original many-body problem by the *auxiliary* problem of non-interacting electrons, assumin that the ground state density of the auxiliary system is the same as the density of the original system [4].

The Hamiltonian of the auxiliary system consists of the kinetic energy term and the effective potential $V^{\sigma}_{eff}(\mathbf{r})$, which is usually chosen to be local:

$$\hat{\mathscr{H}}_{KS} = -\frac{1}{2}\nabla^2 + V^{\sigma}_{eff}(\mathbf{r})$$

The effective potential in general depends on the electron spin σ, however, in this work we will disregard the spin dependence and consider only spin-symmetric case where $N^{\uparrow} = N^{\downarrow}$.

The ground-state density of the KS system is then obtained from the eigenfunctions $\phi_i(\mathbf{r})$ of the KS Hamiltonian:

$$n(\mathbf{r}) = \sum_{i}^{N} |\phi_i(\mathbf{r})|^2$$

According to the second HK theorem, we need the ground state energy fuctional $E[n]$ to find the groud state density of the KS system, which according to the KS ansatz is equal to the true ground state density. This ground state functional of the whole many-body system is written as:

$$E_{KS} = T[n] + \int dr\, V_{ext}(\mathbf{r}) n(\mathbf{r}) + E_{Hartree}[n] + E_{II} + E_{xc}[n] \tag{1.1}$$

where $T[n]$ is the kinetic energy functional of the auxiliary electrons, which can be calculated explicitly as a functional of the KS orbitals:

$$T = \sum_{i}^{N} \langle \phi_i | \nabla^2 | \phi_i \rangle$$

And the Hartree energy $E_{Hartree}$ is the energy of classical charge density $n(\mathbf{r})$ interacting with itself:

$$E_{Hartree}[n] = \frac{1}{2} \int d^3r\, d^3r'\, \frac{n(\mathbf{r}) n(\mathbf{r}')}{|\mathbf{r} - \mathbf{r}'|}$$

The external potential V_{ext} incorporates the potential of the nuclei and other external fields that may be present, and the E_{II} is the energy of the interaction between nuclei.

All terms in the equation (1.1) are well defined, except the last one: the exchange-correlation functional $E_{xc}[n]$. It incorporates all the many-body effects, i.e. electron-electron interaction beyond the classic Hartee term. If the functional $E_{xc}[n]$ was known, we would be able to find the exact ground-state density of the may-body system by finding the minimum of the ground-state energy:

$$\frac{\delta(E^{KS}[n(\mathbf{r})] - \epsilon_i \int d\mathbf{r}\, n(\mathbf{r}))}{\delta n(\mathbf{r})} = 0 \tag{1.2}$$

Which can be rewritten as the Schrödinger-like equation:

$$\left(-\frac{1}{2}\nabla^2 + V_{ext}(\mathbf{r}) + \frac{\delta E_{Hartree}}{\delta\phi_i(\mathbf{r})} + \frac{\delta E_{xc}}{\delta\phi_i(\mathbf{r})}\right)\phi_i = \epsilon_i\phi_i \tag{1.3}$$

This is the Kohn-Sham equation, and it must be solved self-consitently.

While the KS eigenvalues ϵ_i have a definite meaning within the KS theory—Lagrange multipliers in the problem (1.2), they do not have a physical meaning: they are not the electron addition and removal energies, except that in a finite system the highest eigenvalue is equal to the ionization energy. In particular, the KS eigenvalues should not give a correct band gap of a semiconductor.

For the practical implementation of the Kohn-Sham approach the exchange-correlation functional E_{xc} must be approximated. Many functionals have been developed, but for our material (MgO) as well as for many other sp semiconductors and simple metals the most simple, but remarkably useful local density approximation (LDA), which is exact for homogeneous electron gas, shows great results. In LDA, the exchange-correlation energy at each point $\mathbf{r}$ is taken to be equal to the exchange-correlation energy of the homogeneous electron gas with the density at this point. The exchange-correlation energy of the homogeneous electron gas can be calculated with great accuracy using quantum Monte-Carlo methods [5].

To summarise, Kohn-Sham DFT allows us to find the ground state density of the many-body system through the introduction of the auxiliary system of non-interacting electrons. The density we find would be exact if the ground state energy functional $E[n]$ was known. In practice, the kinetic energy, interaction with external potential and Hartree energy are well defined, while the many-body effects are incorporated into the unknown exchange-correlation functional $E_{xc}[n]$; so the density we can calculate is as good as the approximation for the exchange-correlation functional.

In practice, DFT can be successfully applied to many different materials, and can predict ground-state properties—atomic structure, total energy, electronic density, elastic constants, phonon frequencies. For the description of the excited state properties—band gap, optical and dielectric properties etc—one has to go beyond DFT.

1.3 Description of the Spectroscopic Properties

Most generally speaking, spectroscopies measure response of the system to an external perturbation (electromagnetic radiation, fast paricles, etc). We can separate the spectroscopic techniques of interest[1] into two categories: those where the number of particles changes (photoemission and inverse photoemission), and those where the number of particles remains the same (optical absorption, scattering experiments).

In photoemission, the system absorbs a photon and as a consequence emits an electron, which carries certain energy and momentum. From the kinetic energy of the photoelectron, we can find energy

[1]There are many kinds of spectroscopies, and here we will discuss only those where electronic degrees of freedom are involved, like optical absorption, inelastic X-ray scattering, photoemission, and similar.

of the state from which the electron was ejected, and from its direction, we can find the momentum that this electron had inside the crystal. The photoemission experiments probe occupied states of the system. Inverse photoemission probes empty states in the similar fashion: the system is irradiated with a beam of electrons, which couple to the empty states and emit radiation. Description of these spectroscopies relies on the determination of the electron addition and removal energies, and the quasi one-particle picture can be adopted, where the additional particle (the electron or the hole) interacts with the rest of the electrons, which are seen as some effective medium.

In case of neutral excitations, an electron is excited into a higher state, leaving a hole behind; the number of particles in the system remains the same. The electron and the hole interact, screened by the other charged particles, and this interaction cannot be reduced to a one-particle picture. The description of such excitations is different from the description of the charged excitations and is more complicated.

Linear response

If the applied external potential is small, we can consider it as a perturbation and use linear-response framework [6]. The Hamiltonian can be written as: $\hat{\mathscr{H}}(t) = \hat{\mathscr{H}}_0 + \hat{\mathscr{H}}_1(t)$, where $\hat{\mathscr{H}}_0$ is the Hamiltonian of the system in the abscence of external potential, and $\hat{\mathscr{H}}_1$ is the perturbative part. The response function χ relates the perturbing potential[2] to the response of the system:

$$\delta\langle O(\mathbf{r},t)\rangle = \langle O(\mathbf{r},t)\rangle - \langle O(\mathbf{r},t_0)\rangle = \int d\mathbf{r'} \int dt'\, \chi(\mathbf{r},\mathbf{r}';t-t')V(\mathbf{r'},t') \tag{1.4}$$

Where $\langle O(\mathbf{r},t)\rangle$ is the expectation value of the operator O under the perturbing potential V, and the $\langle O(\mathbf{r},t_0)\rangle$ it its expectation value in the unperturbed system. In the $V \to 0$ limit the response function χ is independent of the applied potential. The Fourier transform of the response function is a complex function $\chi(\omega) = \chi_1(\omega) + i\chi_2(\omega)$, and the real and imaginary part are related through Kramers-Kronig relations [3]. The response function which relates induced charge density to the perturbing potential is called *full polarizability*:

$$n_{ind}(\mathbf{r},t) = \int d\mathbf{r'}\, dt'\, \chi(\mathbf{r},\mathbf{r}';t-t')V_{ext}(\mathbf{r'},t') \tag{1.5}$$

It can be shown [6] that the Fourier tranform of polarizability $\chi(\mathbf{r},\mathbf{r'},\omega)$ can be written as:

$$\chi(\mathbf{r},\mathbf{r'},\omega) = \sum_i \left[\frac{f_i(\mathbf{r}) f_i^*(\mathbf{r'})}{\omega - (E_0^N - E_i^N) + i\eta} + \frac{f_i(\mathbf{r'}) f_i^*(\mathbf{r})}{\omega + (E_0^N - E_i^N) + i\eta} \right] \tag{1.6}$$

where $f_i(\mathbf{r}) = \langle N|n(\mathbf{r},0)|N,i\rangle$, and E_0^N and E_i^N are the energies of the ground state $|N\rangle$ and i$^{\text{th}}$ excited state $|N,i\rangle$. It is clear that polarizability has poles at excitation energies of the N-particle system.

The equation (1.6) describes the full polarizability of the system from the microscopic point of view, which is convenient for the microscopic *ab inito* description; however, experiments measure macroscopic, averaged in space quantities.

Microscopic-macroscopic connection

Electrodynamics is able to describe electric and magnetic fields in macroscopic media using the Maxwell equations [7]. The external field induces changes in the system, or, in other words, the external field is screened, which creates induced fields. The total field which acts on a test particle is a sum of the external and induced fields. The quantity which relates induced and external fields is the

[2]The response can be formulated in terms of fields or, alternatively, in terms of potentials; the latter way is easier and thus is perferred.

dielectric function[3]:

$$\mathbf{D}(\mathbf{r},t) = \int d\mathbf{r}'\, dt'\, \epsilon_M(\mathbf{r},\mathbf{r}',t-t')\mathbf{E}(\mathbf{r}',t') \tag{1.7}$$

Where **D** is the electric displacement ("applied field") and **E** is the total electric field. The macroscopic dielectric function $\epsilon_M(\omega) = \epsilon_1 + i\epsilon_2$ is related to the refractive index $n = \sqrt{\epsilon} = \nu + i\kappa$ and other measurable quantities. Absorption coefficient α is proportional to the imaginary part of ϵ_M:

$$\alpha = \frac{\omega\epsilon_2}{\nu c} \tag{1.8}$$

Energy dW lost by fast particle (e.g. electron) due to inelastic scattering in the unit time dt is:

$$\frac{dW}{dt} = -\frac{1}{\pi^2}\int \frac{d\mathbf{k}}{k^2}\Im\left\{\frac{\omega}{\epsilon(\mathbf{k},\omega)}\right\} \tag{1.9}$$

Where the function $\Im\epsilon^{-1}$ is called the *loss function*.

Macroscopic dielectric function ϵ_M only contains information about the way the system reacts to a perturbation on a macroscopic scale, i.e. the scale of the wavelength of applied filed (which in case of UV-VIS spectroscopy is much larger than interatomic distances or the size of the unit cell). We would like to compute ϵ_M from the first principles, e.g. from the quantum mechanical description of the system. The relation between the microscopic response function χ and the experimentally measured quantities is not straightforward. The quantities measured in usual spectroscopy experiments (except atomic resolution electron microscopy and high-energy X-Ray spectroscopy) are averaged over distances which are large comparing to the scale of inhomogenities of the system (unit cell size, interatomic distances, etc) [8]. The response function that we can use to build the bridge between microscopic and macroscopic quantities is the inverse microscopic dielectric function ϵ^{-1}, which is also related to the full polarizability χ:

$$\epsilon^{-1} = \frac{\delta(V_{ext} + V_{Hartree})}{\delta V_{ext}} = 1 + v\chi \tag{1.10}$$

In a periodic solid, it is more convenient to work with the microscopic dielectric function $\epsilon^{-1}(\mathbf{r},\mathbf{r}',\omega)$ in the **k**-space, so it becomes a matrix $\epsilon_{\mathbf{GG}'}(\mathbf{q},\omega)$, where **G** is a reciprocal lattice vector and **q** belongs to the first Brillouin zone: $\mathbf{k} = \mathbf{q} + \mathbf{G}$. The averaging in space is achieved by taking the head element of the matrix:

$$\epsilon_M(\mathbf{q},\omega) = \frac{1}{\epsilon^{-1}_{\mathbf{GG=0}'}(\mathbf{q},\omega)} \tag{1.11}$$

This yields the macroscopic dielectric function ϵ_M, from which we can calculate the quantities relevant to the experiments. Now we will discuss approaches to calculate ϵ^{-1} from the first principles, since from it we can obtain crucial spectrosopic quatities.

1.4 Time-Dependent Density Functional Theory

Runge and Gross extended Hohenberg-Kohn theorems of the density-functional theory to the time domain, showing that the time-evolution of a system is a unique functional of time-dependent density, given the initial wavefunction at one time (when the system begins in its ground state, there is no initial state dependence) [2]. This laid the foundations of the time-dependent density-functional theory (TDDFT), describes the excitations of the many-body system using response functions within Kohn-Sham framework.

[3]This is a function only for isotropic medium or a cubic crystal, and in general case this quantity is a tensor.

The time-dependent Schrödinger-like Kohn-Sham equation is the extension of the equation (1.3):

$$i\hbar\frac{\partial\phi_i(t)}{\partial t} = \left(-\frac{1}{2}\nabla^2 + V_{tot}(\mathbf{r},t)\right)\phi_i(t)$$

with the time-dependent total effective potential:

$$V_{tot}(\mathbf{r},t) = V_{ext}(\mathbf{r},t) + \int dt\,\frac{n(\mathbf{r}',t)}{|\mathbf{r}-\mathbf{r}'|} + V_{xc}[n](\mathbf{r},t) \tag{1.12}$$

where exchange-correlation potential $V_{xc}[n](\mathbf{r},t)$ is the functional of density at all earlier times. It is not known how to create such functional, and in the majority of cases adiabatic approximation is used, where the functional form of the exchange-correlation potential is independent of time.

Here we apply linear response formalism to study the effect of a small perturbation $V_{ext}(\mathbf{r},t)$ on the system using TDDFT. The response function of interest is the full polarizability, introduced in the equation (1.5). We can also introduce the response function χ^0 of the auxiliary non-interacting Kohn-Sham system to the effective total potential (eq. (1.12)):

$$n_{ind}(\mathbf{r},t) = \int d\mathbf{r}\,dt\,\chi^0(\mathbf{r},\mathbf{r}',t-t')V_{tot}(\mathbf{r}',t') \tag{1.13}$$

The independent-particle polarizability χ^0 has a well known form in the frequency domain [8, 6]:

$$\chi^0(\mathbf{r},\mathbf{r}',t-t') = \sum_{vc}\frac{\phi_v^*(\mathbf{r})\phi_c^*(\mathbf{r})\phi_c^*(\mathbf{r}')\phi_v(\mathbf{r}')}{\omega-(\epsilon_c-\epsilon_v)-i\eta} \tag{1.14}$$

The two response functions χ and χ^0 are related through a Dyson-like equation:

$$\chi(\mathbf{r},\mathbf{r}',\omega) = \chi^0(\mathbf{r},\mathbf{r}',\omega) + \int\int d\mathbf{r}''\,d\mathbf{r}'''\left(\chi^0(\mathbf{r},\mathbf{r}',\omega)\left(v(\mathbf{r}'',\mathbf{r}''') + f_{xc}(\mathbf{r}'',\mathbf{r}''',\omega)\right)\chi(\mathbf{r}''',\mathbf{r}',\omega)\right)$$

or, using concise notation:

$$\chi = \chi^0 + \chi^0(v+f_{xc})\chi \tag{1.15}$$

where $v = \delta V_{Hartree}/\delta n$, and $f_{xc} = \delta V_{xc}/\delta n$ is the *exchange correlation kernel*, which accounts for the first order exchange and correlation effects in the perturbing potential.

For homogeneous systems, heterogenities due to the local structure—local field effects—can be neglected:

$$n(\mathbf{r},t) = \int\int dt\,d\mathbf{r}'\,\chi(\mathbf{r}-\mathbf{r}',t-t')V_{ext}(\mathbf{r}',t')$$

In the reciprocal space the polarizability matrix $\chi_{\mathbf{GG}'}(\mathbf{q},\omega)$ becomes diagonal. Of course, realistic systems are not homogeneous, and care must be taken when the local fields are not taken into account. This approximation might have a small effect in simple solids, but fails completely in heterostructures and finite systems, where the off-diagonal elements cannot be neglected.

In practice, the calculation of optical spectra in TDDFT is done in the following way:

1. Ground state calculation of the Kohn-Sham wavefunctions ϕ_i and eigenenergies ϵ_i.
2. Calculation of the independent-particle polarizability χ^0 from the KS wavefunctions and eigenvalues according to the equation (1.14).
3. Calculation of the full polarizability χ using the equation (1.15).
4. Calculation of the inverse microscopic dielectric function ϵ^{-1} (eq. (1.10))
5. Finally, the macroscopic dielectric function ϵ_M (eq. (1.11)), from which the absorption, energy loss and other spectra can be obtained.

To calculate the full polarizability χ, we need the exhange-correlation kernel, which is not known and must be approximated. The simplest way is the random phase approximation (RPA) [9], in

which the exchange-correlation kernel is simply neglected: $f_{xc}^{RPA} = 0$. This means that the exchange-correlation effects are taken into account only during KS DFT ground state calculation, but are neglected in the caclulation of the linear response. In fact, the polarizability obtained with RPA is equivalent to the application of Fermi Golden Rule to the Kohn-Sham system of noninteracting particles, if no local fields are included. The other common approximation is the adiabatic local density aproximation (ALDA), which sets the exchange-correlation kernel equal to the functional derivative of the LDA exchange-correlation potential V_{xc}^{LDA} with respect to the density n in adiabatic (i.e. static, time-independent) limit:

$$f_{xc}^{ALDA}(\mathbf{r}, \mathbf{r}') = \delta(\mathbf{r} - \mathbf{r}') \frac{\delta V_{xc}^{LDA}(n(\mathbf{r}))}{\delta n(\mathbf{r})} \tag{1.16}$$

In the adiabatic approximation all the memory effects are neglected, and the kernel is time-independent. ALDA gives satisfactory EELS and also optical spectra for finite systems (molecules and clusters), but systematically fails to describe optical spectra of solids [10]. To describe them other approximations for the f_{xc} are developed [11, 12]; however, state of the art description of the optical properties is done within the Green's funciton formalism.

1.5 Green's function formalism

Density funcitonal theory, discussed in the previous sections, uses electronic density n as a basic variable. While this is an integrated variable which does not contain as much information about the system as the many-body wavefunction, it is exteremely useful for finding the quantities that are interesting from the practical point of view. Another integrated variable of such kind is a one-particle Green's function, which can be interpreted as a frequency-dependent one-particle density matrix. The one-particle Green's function contains information about single-particle addition and removal energies, expectation values of single-particle operators, and ground state energy of the system. It is especially useful for description of photoemission experiments. While in this work photoemission is not the subject of interest, introduction of the single-particle Greens' function is the necessary step for us to come to the two-particle Green's functions, which are invaluable for the description of electron-hole pairs.

The Green's functions are defined within the second quantization formalism. The key concepts of the second quantisation are creation and annihilation operators $\hat{c}_i^\dagger$ and $\hat{c}_i$, which create (and annihilate, respectively) a particle in the state ϕ_i. They can be represented in the position basis of eigenfunctions of the x-operator (where x stands for the spatial and spin coordinates $(\mathbf{r}, \sigma)$), in which case they are called field operators $\hat{\psi}^\dagger(x)$ and $\hat{\psi}(x)$. If the operator $\hat{c}_i^\dagger$ creates a particle in the state ϕ_i, the operator $\hat{\psi}^\dagger(x)$ creates a particle with the coordinate x, i.e. with spin σ and in the position $\mathbf{r}$.

Now, for a many-body system with the N-particle ground state $|N\rangle$ and field operators in Heisenberg picture $\hat{\psi}(1)$ and $\hat{\psi}^\dagger(2)$ (where (1) is the shorthand for $(\mathbf{r}_1, \sigma_1, t_1)$) we can define the single particle Green's function [13, 6]:

$$iG(1,2) = \begin{cases} \langle N|\hat{\psi}(1)\hat{\psi}^\dagger(2)|N\rangle, & \text{if } t_1 > t_2 \\ \langle N|\hat{\psi}^\dagger(2)\hat{\psi}(1)|N\rangle, & \text{if } t_1 < t_2 \end{cases}$$

The Green's function describes propagation of a particle added to a system at time t_1 and coordinate r_1, and removed from the system at the time t_2 and coordinate r_2. If $t_1 > t_2$, the Green's funtion describes propagation of a hole, and if $t_1 < t_2$, it describes proparagion of an electron.

In the Lehmann representation, Green's function in the frequency space can be written as [6]:

$$G(\mathbf{r}_1, \mathbf{r}_2, \omega) = \sum_i \frac{f_i(\mathbf{r}_1) f_i^* \mathbf{r}_2}{\omega - \epsilon_i + i\eta \,\mathrm{sign}(\epsilon_i - \mu)} \tag{1.17}$$

where $\epsilon_i = E_{|N\rangle} - E_{|N+1,i\rangle}$, μ is chemical potential, and $f_i(\mathbf{r})$ are the Lehmann amplitudes:

$$f_i(\mathbf{r}) = \begin{cases} \langle N|\hat{\psi}(\mathbf{r})|N-1,i\rangle, & \text{if } \epsilon_i > \mu \\ \langle N-1,i|\hat{\psi}(\mathbf{r})|N\rangle, & \text{if } \epsilon_i < \mu \end{cases}$$

In the Lehmann representation it becomes clear that $G(1,2)$ has poles at the particle addition and removal energies, which lay infinitesmally below real axis if $\epsilon_i > \mu$, and infinitesmally above it if $\epsilon_i < \mu$. This makes it the ideal tool to describe charged excitations and photoemission spectroscopies.

The formal definition of Green's function is useless from the practical point of view, as it is based on the full many-body wavefunction $|N\rangle$. One of the approaches to calculate Green's function is a perturbative approach, adopted by Many-Body Perturbation Theory. The other way is to find an equation for which Green's function is a solution, and solve it approximately.

From the equations of motion for the field operators in Heisenberg picture, it is possible to derive the hierarchy of the equations of motion for the Green's functions:

$$\left[i\frac{\partial}{\partial t} - h_0(\mathbf{r}_1)\right] G(1,2) = \delta(1,2) - i\int d3\, v(1,3) G_2(1,3^+;2,3^{++})$$

where $3^+ = (\mathbf{r}_3, \sigma_3, t_3 + \delta)$, δ being a positive infinitesmal. This equation establishes relation between one-particle Greens function G and the two-particle Green's function G_2. The 2-paricle Greens function is then related to the 3-particle Green's function, and so on, untill the full many-body Green's function. The fundamental idea is that if one is interested in one-particle properties, one needs only one-particle Green's function. By making approximations to the Green's functions for higher number of particles, we can solve this equation of motion and obtain approximated 1-particle Green's function. For example, making independent particle approximation for the 2-particle Green's function yields the 1-particle Green's Function in the Hartree-Fock approximation.

Alternatively, we can introduce the self-energy operator, in which the higher-order excitations are folded:

$$\left[i\frac{\partial}{\partial t} - h_0(\mathbf{r}_1) - V_{Hartree}(1)\right] G(1,2) = \delta(1,2) - i\int d3\, \Sigma(1,3) G(3,2) \tag{1.18}$$

It is a complex non-local frequency-dependent operator, which implicitly takes into account many-body effects (exchange and correlation) of the system.

The independent-particle[4] Green's function $G^0(1,2)$ is obtained by setting $\Sigma = 0$:

$$\left[i\frac{\partial}{\partial t} - h_0(\mathbf{r}_1) - V_{Hartree}(1)\right] G^0(1,2) = \delta(1,2)$$

Inserting the definition of the G^0 into the equation of motion (1.18) yields the Dyson equation:

$$G(1,2) = G^0(1,2) + \int d(34)\, G^0(1,3)\Sigma(3,4)G(4,2)$$

or, using the concise symbolic notation:

$$G = G^0 + G^0 \Sigma G. \tag{1.19}$$

Single-particle Green's function is the resolvent of a Schrödinger-like equation:

$$\left[\frac{1}{2}\nabla^2 + V_{ext}(\mathbf{r}) + V_{Hartree}(\mathbf{r})\right]\Psi_i(\mathbf{r}) + \int d\mathbf{r}'\, \Sigma(\mathbf{r},\mathbf{r}',\omega)\Psi_i(\mathbf{r}',\omega) = E_i(\omega)\Psi_i(\mathbf{r},\omega) \tag{1.20}$$

[4]Even though the Green's funciton $G^0(1,2)$ is called "non-interacting", it still contains Hartree potential.

which can be approximated by putting $\omega = E_i(\omega)$, giving rise to the *quasiparticle equation* (which is equavalent to assuming that the complex pole of G is its dominant part).

The concept of quasiparticles was introduced by Lev Landau in the Fermi liquid theory. He noticed that in the liquid, instead of considering electrons interacting via the long-range Coulomb forces, we can consider quasiparticles (or "dressed" eletrons), which interact via short-ranged, screened interaction. Any electron excludes the other electrons from its neighborhood, and thus effectively carries around itself a cloud of positive charge. While such electron requires a very complicated description, if we consider the electron with its cloud as a quasiparticle, which weakly interacts with other quasiparticles, the description becomes much more simple. Such quasiparticle has the same spin, charge and momentum, but dynamical properties (mass, magnetic momentum etc) are renormalized. As the quasiparticles are not the eigenstates of the system, they can dissipate and break down, and the farther they are from the Fermi surface, the shorter is their lifetime. All the difference between bare electrons and quasiparticles is incorporated into the self energy, whcih is non-local, frequency-dependent, non-hermitian operator.

The quasiparticles near Fermi surface are very similar to the non-interacting (but still subjected to the Hartree potential) electrons, and so the properties of the Fermi liquid near Fermi surface can be derived using perturbative approach, slowly switching the interaction on. One can also notice that the Kohn-Sham equation (1.3) is similar to the quasiparticle equation (1.20), where $V_{xc}(\mathbf{r})$ plays the role of self energy $\Sigma(\mathbf{r}$. This is the reason why the Kohn-Sham DFT yields good band dispersion for most materials: if the quasiparticle picture is reasonable, the LDA Kohn-Sham orbitals are often close to the quasiparticle states. There are cases, however, when quasiparticle picture is invalid; in this case, the whole concept of band structure becomes meaningless, and one has to be careful with the interpretation of the results of band structure calculations.

1.6 GW approximation

Lars Hedin in 1965 developed the approach to approximate the self-energy Σ [14]. He derived 5 coupled integro-differential equations, cast in terms of a 1-particle Green's function G, self-energy Σ, irreducible polatizability $\tilde{P}$, screening W and vertex Γ, which are often called "Hedin's pentagon":

$$\Sigma(1,2) = i \int d(34)\, G(1,3)\Gamma(3,2,4)W(4,1^+) \tag{1.21}$$

$$G(1,2) = G^0(1,2) + \int d(34) G^0(1,3)\Sigma(3,4)G(4,2) \tag{1.22}$$

$$\Gamma(1,2,3) = \delta(1,2)\delta(1,3) + \int d(4567)\, \frac{\delta\Sigma(1,2)}{\delta G(4,5)} G(4,6)G(7,5)\Gamma(6,7,3) \tag{1.23}$$

$$W(1,2) = v(1,2) + \int d(34) v(1,3)\tilde{P}(3,4)W(4,2) \tag{1.24}$$

$$\tilde{P} = -i \int d(34)\, G(1,3)G(4,1^+)\Gamma(3,4,2) \tag{1.25}$$

The irreducible polarizability is defined as:

$$\tilde{P} = \frac{\delta n(1)}{\delta U(2)}, \qquad \text{where } U(2) = V_{ext}(2) + V_H(2) \tag{1.26}$$

The vertex function is:

$$\Gamma(1,2,3) = -\frac{\delta G^{-1}(1,2)}{\delta U(3)} = \delta(1,2)\delta(1,3) + \frac{\delta\Sigma(1,2)}{\delta U(3)} \tag{1.27}$$

And through the definition of the time-ordered dielectric function:

$$\epsilon(1,2) = \delta(1,2) - \int d3\, v(1,3)\tilde{P}(3,2) \tag{1.28}$$

we can obtain the equation for the screening:

$$W(1,2) = \int d3\, \epsilon^{-1}(3,2)v(1,3) \tag{1.29}$$

The five Hedin's equations are exact, and in principle, they could be solved in an iterative way; however, in practice this is not possible, and some approximations must be made.

The GW approximation [14, 15] neglects the variation of self-energy in the equation for vertex function (1.23), making $\Gamma^{GW}(1,2,3) = \delta(1,2)\delta(1,3)$. Now, to solve the Hedin's equation, we start from setting the Green's function equal to the G^0, and the other equations become:

$$\begin{aligned} P^0(1,2) &= -iG^0(1,2)G^0(2,1+) \\ W^0(1,2) &= v(1,2) + \int d(34)\, v(1^+,3)P^0(3,4)W^0(4,2) \\ \Sigma(1,2) &= iG^0(1,2)W^0(1+,2) \end{aligned}$$

The polarizability P^0 is the independent-particle RPA polarizability. Using the obtained self-energy $\Sigma^0 = G^0W^0$, we can obtain quasiparticle energies from the equation (1.20). As was mentioned before, the Kohn-Sham equation is similar to the quasiparticle equation, and so we can treat the difference as a perturbation. This is why the GW corrections are calculated on top of the KS DFT results. One can solve the Hedin's equations in GW approximation in a self-consistent way with both energy and wavefunctions, or stop at the first-order corrections to the KS energies (so called G^0W^0); there are also intermediate approaches, for instance, G^0W, GW^0 and so on.

GW approximation describes the propagation of the additional particle (electron or hole) in the effective medium, replacing the many-body interactions between additional charge and the electrons with the polarizability of the medium. In fact, GW approximation is the Hartree-Fock approximation with an additional term: the screened Coulomb interaction. Comparing to the Hartree-Fock approximation, where potential has infinite range and is static, the screened Coulomb interaction W is dynamic (and in metallic systems also short-ranged). Because of the frequency dependence of the self-energy, we can obtain more solutions than the dimention of a basis (more, than there are particles in a system), which is impossible in adiabatic approximation to the kernel. In case of GW, this means that we take into account coupling of the additional particle with plasmons [16]. The GW approximation, however, is reliable only when this coupling is weak.

The GW approximation is good for the description of photoemission experiments and yeilds bandgap energies very close to experiment [17]. However, it fails at the description of optical properties, because the variation of self-energy in eq. (1.23), neglected in the GW approximation, contains the information about electron-hole interaction, which is essential for the description of neutral excitations. This variation enters the kernel of the Bethe-Salpeter equation for the 2-particle Green's funciton, which allows for a state of the art description of the optical properties, including the excitonic effects.

1.7 Bethe-Salpeter equation

The optical absorption inevitably involves interaction between the electron in an excited state and the hole it left behind in a valence state. It cannot be described within one-particle picture, as the electron-hole interaction must be taken into account. Thus, we introduce the two-particle Green's

function [6]:

$$G(1,2,3,4) = (-i)^2\langle N|\mathcal{T}\left[\hat{\psi}(1)\hat{\psi}(3)\hat{\psi}^\dagger(4)\hat{\psi}^\dagger(2)\right]|N\rangle$$

The two-particle excitations are described using the two-particle correlation function L, also called four-point polarizability:

$$L(1,2,3,4) = L^0(1,2,3,4) - G(1,2,3,4),$$

where the independent-particle polarizability L^0 describes the propagation of an electron and a hole that don't interact: $L^0(1,2,3,4) = iG(1,3)G(4,2)$. The four-point polarizability L enters the Dyson-like equation, known as the *Bethe-Salpeter equation* [18]:

$$L(1,2,3,4) = L^0(1,2,3,4) + \int d(5678)L^0(1,2,5,6)\left[v(5,7)\delta(5,6)\delta(7,8) + \Xi(5,6,7,8)L(7,8,3,4)\right],$$

where the kernel Ξ is:

$$\Xi(5,6,7,8) = i\frac{\delta\Sigma(5,6)}{\delta G(7,8)}$$

The four-point polarizability L can be contracted to obtain the two-point response function $\chi = \delta n(1)/\delta V_{pert}(2)$:

$$\chi(1,2) = L(1,1^+,2,2^+)$$

The many-body kernel Ξ is unknown, and must be approximated. Setting $\Sigma_x(1,2) = iG(1,2)v(1,2)$ (i.e. neglecting screening) yields the time-depentent Hartree-Fock approximation, while the "standard" Bethe-Salpeter equation implies the use of GW self-energy:

$$\Xi(5,6,7,8) = i\frac{\delta\Sigma^{GW}(5,6)}{\delta G(7,8)} = -\frac{\delta G(5,6)W(5,6)}{\delta G(7,8)} = W(5,6)\delta(5,7)\delta(7,8) + G(5,6)\frac{\delta W(5,6)}{\delta G(7,8)}$$

Here the term $G\delta W/\delta G$ describes a second-order effect —the change in screening because of the excitation, and is normally neglected. The Behte-Salpeter equation finally becomes:

$$\begin{aligned} L(1,2,3,4) &= L^0(1,2,3,4) \\ &+ \int d(5678)\, L^0(1,2,5,6)\left[v(5,7)\delta(5,6)\delta(7,8) - W(5,6)\delta(5,7)\delta(6,8)\right] L(7,8,3,4) \end{aligned}$$

or, using concise notation, $L = L^0 + L^0[v - W]L$.

The Bethe-Salpeter equation describes the response to a perturbation as creation of electron-hole pairs, which is expressed by the term L^0. The electron-hole pairs, in turn, create the induced potential, which affects the rest of the system, modifying the potential which acts on the electon-hole pair in a self-consistent manner. This two-particle picture allows for the description of excitonic effects in spectra, including the formation of bound excitons.

Dynamical effects in W and in G tend to cancel out in case of simple semiconductors, so they are usually neglected in both. This means that the screening is assumed to be instanteneous. Including the dynamical effects in the interactions would give rise to a non-Hermitian kernel, which would allow us to describe, among other effects, excitonic lifetimes, double excitations, dynamical screening etc.However, there is no practical implementation of the dynamic BSE so far, and the statec BSE is considered to be the state of the art for electronic structure response functions.

Chapter 2

Computations

All methods that we use are fully *ab initio*, meaning that there are no adjustable parameters, and everything is calculated from the first principles. The only parameters we have are the convergence parameters, which must me changes untill the spectrum (or other quantity of interest) does not change anymore.

2.1 Structure of MgO

MgO (periclase) has rock salt crystal structure, with 2 atoms in a unit cell: Mg at the position (0, 0, 0) and O at the position (1/2, 1/2, 1/2) is the reduced coordinates. The lattice constant as measured my the X-ray diffraction is 4.217 Å [19].

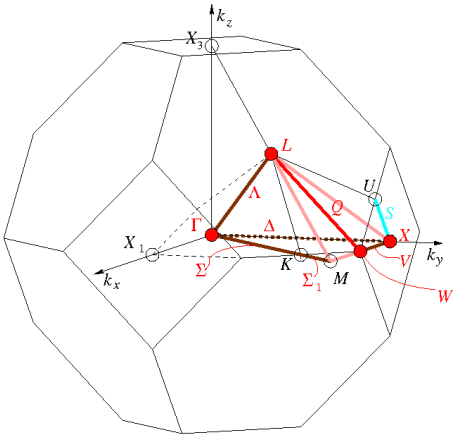

Figure 2.1: First Brillouin zone of a face-centered cubic crystal (space group 225). The scheme was taken from the Bilbao crystallographic server [20]

Special point	reciprocal coordinates	cartesian coordinates
Γ	0, 0, 0	0, 0, 0
X	1/2, 1/2, 0	0, 0, 1
L	1/2, 1/2, 1/2	1/2, 1/2, 1/2
W	1/2, 3/4, 1/4	1/2, 0, 1
K	3/8, 3/8, 3/4	3/4, 3/4, 0

Table 2.1: Coordinates of the special points in the first Brillouin zone of fcc crystal. [20]

The Brillouin zone of the face-centered cubic crystal is presented on the Fig. 2.1. The coordinates of symmetry points are listed in the Table 2.1. These coordinates were used in the calculation of band structure and of the loss properties for $\mathbf{q} > 0$.

2.2 DFT calculations

The DFT calculations were performed using Abinit code [21] with local density approximation. The Kohn-Sham (KS) equation (1.3) must be solved in the iterative way to find the KS wavefunctions ϕ_i and eigenenergies ϵ_i.

The number of iterations is determined by the difference between the wavefunctions, or between total energies that are obtained between iterations.

For periodic solids, it is convenient to work in a reciprocal space, so the plane wave basis set is a natural choice:

$$\psi_{n\mathbf{k}}(\mathbf{r}) = e^{i\mathbf{k}\cdot\mathbf{r}} u_{n\mathbf{k}}(\mathbf{r}), \qquad \text{where} \qquad u_{n\mathbf{k}}(\mathbf{r}) = \sum_{\mathbf{G}} u_{n\mathbf{k}}(\mathbf{G}) e^{i\mathbf{G}\cdot\mathbf{r}} \tag{2.1}$$

The size of the basis set is determined by the number of $\mathbf{G}$ vectors, included in the sum (2.1). This number is usually specified indirectly, using the *energy cutoff*:

$$\frac{(\mathbf{k}+\mathbf{G})^2}{2} < E_{cut} \tag{2.2}$$

Many quantities that we calculate require integration over the Brillouin zone. To compute such integrals numerically, we have to convert integral to a sum over the set of k-points. It turns out that some ways to sample the Brillouin zone are better than the other. Monkhorst and Pack presented a way to build k-point grids which ensure fast convergence [22], and we follow this recipe for our DFT calculations.

We use pseudopotential approach [23] which allows us to exclude core electrons form the calculations [3] and thus reduce the computation cost. The pseudopotentials we used were the norm-conserving Troullier-Martins taken from the Abinit web site [24].

2.3 TDDFT calculations

The general scheme of TDDFT calculations was presented in the section 1.4. The Kohn-Sham energies and wavefunctions (computed in the previous step) enter the equation (1.14) for χ^0, which through the eq. (1.15) and (1.10) leads to the microscopic dielectric matrix $\epsilon_{\mathbf{GG'}}(\mathbf{q},\omega)$. The head element of the matrix is then inverted to obtain the macroscopic dielectric function ϵ_M (eq. (1.11)).

We have performed the computations using DP code [25] with RPA and ALDA. The most important parameters that enter the calculations are: number of bands to sum over in the equation (1.14) for χ_0; size of the plane wave basis set; number of the $\mathbf{G}$ vectors, i.e. dimention of the $\epsilon_{\mathbf{GG'}}(\mathbf{q},\omega)$ matrix.

The k-point grid used for the calculation of optical properties is different from the symmetric Monkhorst-Pack grids. For fast convergence of optical spectra the grid must contain no high-symmetry points. It is built in a similar way to a Monkhorst-Pack grid, except that the shifts are symmetry-breaking [26].

2.4 G^0W^0corrections in practice

The GW corrections were performed with Abinit code [27] using plasmon-pole model.

The independent-particle Green's function is built from the Kohn-Sham wavefunctions and energies. The polarizability which is required for calculation of screening is independent-particle RPA polarizability χ^0, which in k-space is:

$$\chi^0_{\mathbf{GG'}}(\mathbf{q},\omega) = \frac{2}{\Omega}\sum_{\mathbf{k}}^{BZ}\sum_{\mathrm{cv}} \frac{\tilde{\rho}^t\tilde{\rho}^{t*}}{\omega + \epsilon_{\mathrm{c},\mathbf{k}-\mathbf{q}} - \epsilon_{\mathrm{v},\mathbf{k}} - i\eta} + \frac{2}{\Omega}\sum_{\mathbf{k}}^{BZ}\sum_{\mathrm{cv}} \frac{\tilde{\rho}^t\tilde{\rho}^{t*}}{\omega - (\epsilon_{\mathrm{c},\mathbf{k}-\mathbf{q}} - \epsilon_{\mathrm{v},\mathbf{k}}) - i\eta} \tag{2.3}$$

where the matrix elemets $\tilde{\rho}^t$ for each transition t between states $|\mathbf{k}\text{-}\mathbf{q},\mathrm{c}\rangle$ and $|\mathbf{k},\mathrm{v}\rangle$ are:

$$\tilde{\rho}^t = \langle \mathbf{k}\text{-}\mathbf{q},\mathrm{c}|e^{-i(\mathbf{q}+\mathbf{G})\mathbf{r}}|\mathbf{k},\mathrm{v}\rangle = \sum_{\mathbf{G'}} u^*_{\mathbf{k}-\mathbf{q},\mathrm{c}}(\mathbf{G'}) u^*_{\mathbf{k},\mathrm{v}}(\mathbf{G}+\mathbf{G'}) \tag{2.4}$$

The crucial parameters are: dimetions of matrix $\chi^0_{\mathbf{GG}}$, (eq. (2.3)); number of bands to sum over

(eq. (2.3)); number of k-points to sum over (eq. (2.3)); size of the basis set (number of **G** vectors, equation (2.4)).

Next, the quasiparticle energies must be computed using the G^0W^0self-energy:

$$\Sigma(\mathbf{r}, \mathbf{r}', \omega) = \frac{i}{2\pi} \int d\omega' \, G^0(\mathbf{r}, \mathbf{r}', \omega - \omega') W^0(\mathbf{r}, \mathbf{r}', \omega) e^{-i\eta\omega'} \tag{2.5}$$

where W^0 is the screened Coulomb interaction calcualted with χ^0. Since the quasiparticle equation (1.20) is similar to the KS equation (1.3), it is reasonable to assume that $\phi_i^{QP} \approx \phi_i^{KS}$, and so the equation for quasiparticle energies becomes:

$$\epsilon_i^{QP} = \epsilon_i^{KS} + \langle \phi_i^{KS} | \Sigma(\mathbf{r}, \mathbf{r}', \omega = \epsilon_i^{QP}) - V_{xc}(\mathbf{r}) | \phi_i^{KS} \rangle \tag{2.6}$$

The self-energy depends on the energy, and so the equation (2.6) should be solved self-consistently. However, in practice the self-energy is linearized:

$$\langle \Sigma(\omega = \epsilon_i^{QP}) \rangle = \langle \Sigma(\omega = \epsilon_i^{KS}) \rangle + (\epsilon_i^{QP} - \epsilon_i^{KS}) \langle \frac{\partial \Sigma(\omega)}{\partial \omega} |_{\omega = \epsilon_i^{KS}} \rangle \tag{2.7}$$

The matrix elements of $\Sigma(\omega)$ are computed in the basis of KS wavefunctions. The self-energy is divided into exchange part, which is frequency indepenent, and correlation part, which is dynamic. The frequency dependence of $\Sigma_c(\omega)$ comes from the W^0, and can be approximated with *plasmon-pole model* [28] using two *ab initio* calculated ω points.

The calculation of $\langle \Sigma_c(\omega) \rangle$ is the most CPU-demanding part of the computation. It involves double summation over **G** vectors and tends to converge very slowly with the number of bands.

2.5 Solving Bethe-Salpeter equation

We used EXC code to solve Bethe-Salpeter equation [29]. To solve the Bethe-Salpeter equation (1.7) numerically, we must work in the basis of independent-particle transitions:

$$L(1234, \omega) \Rightarrow L_{n_1 n_2}^{n_3 n_4}(\omega) = \int d(1234) \, L(1234, \omega) \phi_{n1}(\mathbf{r}) \phi_{n_2}^*(\mathbf{r}) \phi_{n_3}(\mathbf{r}') \phi_{n_4}^*(\mathbf{r}') \equiv \langle\langle L \rangle\rangle \tag{2.8}$$

The BSE can be rewritten in the transition space:

$$L_{n_1 n_2}^{n_3 n_4}(\omega) = \Big[(\epsilon_{n_2}^{QP} - \epsilon_{n_1}^{QP} - \omega) \delta_{n_1 n_3} \delta_{n_2 n_4} + \langle\langle v \rangle\rangle + \langle\langle W \rangle\rangle \Big]^{-1} = [H^{exc} - \omega]^{-1} \tag{2.9}$$

where ϵ_n^{QP} are the quasiparticle energies, which leads us to the excitonic Hamiltonian:

$$H^{exc} = \Big[(\epsilon_{n_2}^{QP} - \epsilon_{n_1}^{QP}) \delta_{n_1 n_3} \delta_{n_2 n_4} + \langle\langle v \rangle\rangle + \langle\langle W \rangle\rangle \Big] \tag{2.10}$$

The eigenfunctions A_λ and eigenvalues E_λ of this Hamiltonian let us obtain the ϵ_M:

$$\epsilon_M = 1 - \frac{8\pi}{q^2} \sum_\lambda \frac{|\sum_t A_\lambda^t \tilde{\rho}^t|^2}{\omega - E_\lambda + i\eta} \tag{2.11}$$

where the sums runs over all independent-particle transitions t and over all excitonic states λ.

There are two ways to obtain the spectrum form the H_{exc}. First, it can be fully diagonalized, in which case we obtain A_λ and E_λ; second, L can be partially inverted using iterative alogithms [30], which allows us to obtain ϵ_M bypassing the A_λ and E_λ. Full diagonalization thus gives more information, but it is much more memory and CPU demanding; the iterative inversion allows us to tackle much larger systems with more bands, and thus obtain spectrum in a wider energy range.

Chapter 3

Results

3.1 Ground state calculations and band structure

At first, we have to calculate the ground state density of MgO, which we do using the trusted DFT method. The main purpose of the DFT calculations in this work is to obtain the Kohn-Sham wavefunctions and eigenenergies, which enter the calculation of the independent-particle polarizability χ^0. We also calculated the Kohn-Sham band structure, and density of states, which carry a lot of useful information about the electronic structure of the material.

We use LDA approximation for the DFT calculation. We verified that LDA results differ very little from the results obtained with generalized gradient approximation (GGA), data not shown. To get an evidence that the LDA indeed works well, we calculated the lattice constant[1]. For this, we performed self-consisted DFT calculation of the total energy at different values of the lattice constant, and fit the obtained values to parabola (Fig. 3.1). The position of the minimum of this parabola gave us the equilibrium value of the lattice constant: 4.242 Å. The experimental value is 2.217 Å, so the discrepancy is 0.6%. This agreement is very good, and is a sign that the ground state density that we calculated within the LDA is close to the real one.

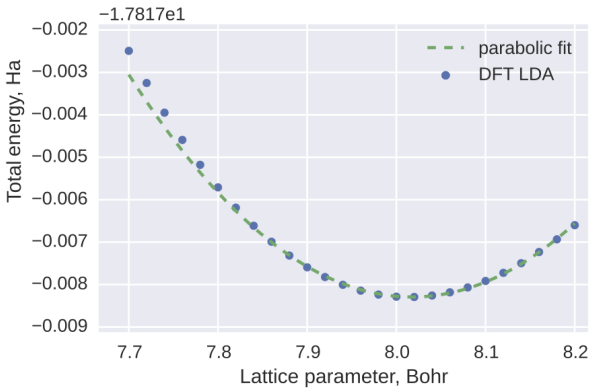

Figure 3.1: Total energy per unit cell as a function of a lattice constant for MgO, calculated within the local density approximation of DFT. The dependence is close to the parabolic fit near the equilibrium, but becomes more steep for lower values of the lattice constant.

The calculated band structure of MgO is shown on the Figure 3.2a. The LDA band gap is equal to 4.62 eV, it is direct and located at Γ point. The experimental band gap is 7.8 eV [31], and the calculated value is a severe underestimation. This is expected from the LDA DFT, as it is known to underestimate bandgaps of solids. To correct the value of the bandgap, we performed G^0W^0corrections, which are described later.

As we use a pseudopotential approach [23], only valence electrons (2 from Mg and 6 from O per unit cell) are taken into account during the calculation. The 8 electrons of the unit cell fill 4 valence bands. The lowest valence band is almost flat and is about 12 eV lower than the other three valence bands, which all lie close in energy and have a dispersion of about 4 eV. The Γ point is triply degenerate, which is typical for face-centered cubic crystals. The two highest bands (3rd and 4rth) are degenerate along some directions, in particular, along Γ-L and Γ-X. The dispersion of the bands

[1] MgO has the face-centered cubic crystal (fcc) structure, so the only parameter that is necessary to describy crystal geometry is the lattice constant; see also section 2.1

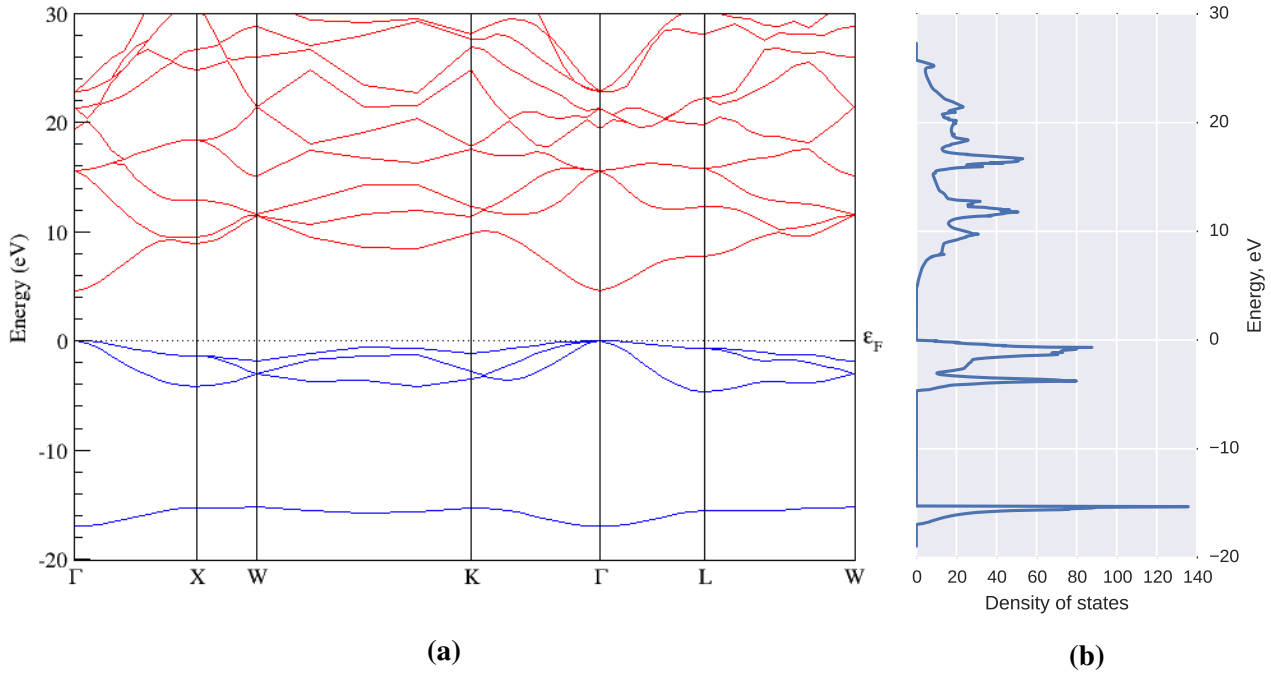

Figure 3.2: (a) LDA band structure of MgO. (b) The total density of states.

in the vicinity of the Γ point has parabolic character. The curvature of the valence bands determines effective mass of the holes, and as a consequence, their mobility. As the bands are triple degenerate and non-isotropic, the effective mass is a tensor, and finding it is a non-trivial task, which we did not pursue.

The lowest conduction band is non-degenerate at Γ, and the gap at Γ is much smaller than the gap at other points.

The projected density of states (pDOS) (Fig. 3.3) shows that the lowest valence band is formed by the s-orbitals of Oxygen, and the three other valence bands are the p-states of Oxygen. The electronic density is virtually absent on the Magnesium, showing that the bond character is strongly ionic. The conduction bands have mixed character with the strongest contribution from the p-states of Oxygen.

3.2 Optical properties with TD DFT

In opder to evaluate optical properties of MgO, we start from TDDFT fro it is in principle much simpler and in practice much faster and less memory demanding. We calculated the real ϵ_1 and imaginary ϵ_2 part of the macroscopic dielectric function ϵ_M in the random-phase approximation (RPA) and adiabatic local-density approximation (ALDA) of TD DFT following equations (1.14), (1.15) and (1.10). The results are shown on the Figure 3.4, together with the experimentally obtained dielectric function [31]. The RPA results are very similar to the ALDA, and the disagreement with the experiment is striking. First of all, the absorption edge is red-shifted: while in principle the band gap underestimation must be cured by the exchange-correlation kernel f_{xc}, both approximations for the f_{xc} that we used cannot handle this problem (see also section 1.4). Second, the sharp peak in the ϵ_2 given by the bound exciton is absent, and the spectral weight is blue-shifted. This is because electron-hole interaction is not taken into account in the approximations from f_{xc}, and so the excitonic effects are absent.

We also studied the importance of crystal local field effects for the description the macroscopic dielectric function. As can be seen on the Figure 3.5, there is no significant difference between the curves with and without local fields, and so the non-diagonal elements of the microscopic dielectric function $\epsilon_{\mathrm{GG}'}$ can be neglected.

As there is no improvement in going from RPA to ALDA, and including the local field effects

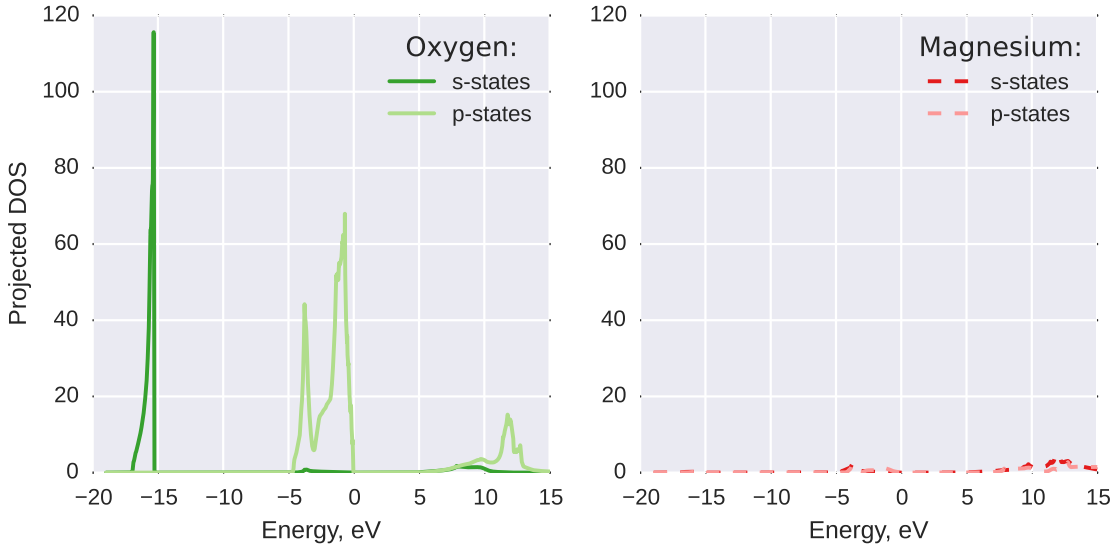

Figure 3.3: The projected density of states for s and p states of Magnesium (right) and Oxygen (left). Virtually all electronic density is located at the Oxygen, so the bond character is strongly ionic.

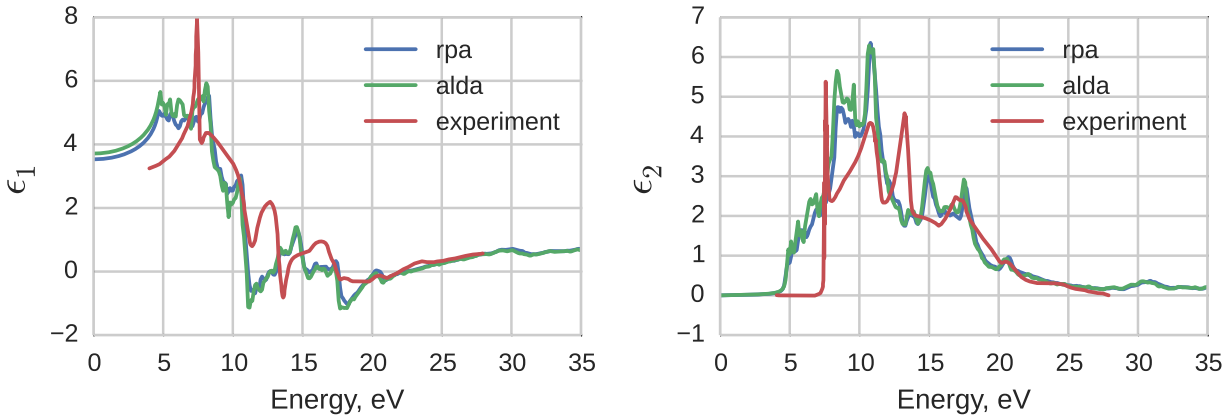

Figure 3.4: Real and imaginary part of the dielectric function calculated with random phase approximation (RPA) and adiabatic local density approximation (ALDA) of TDDFT, compared to the experimental data [31]. Both approximations yield dielectric function ϵ which poorly agrees with the experiment.

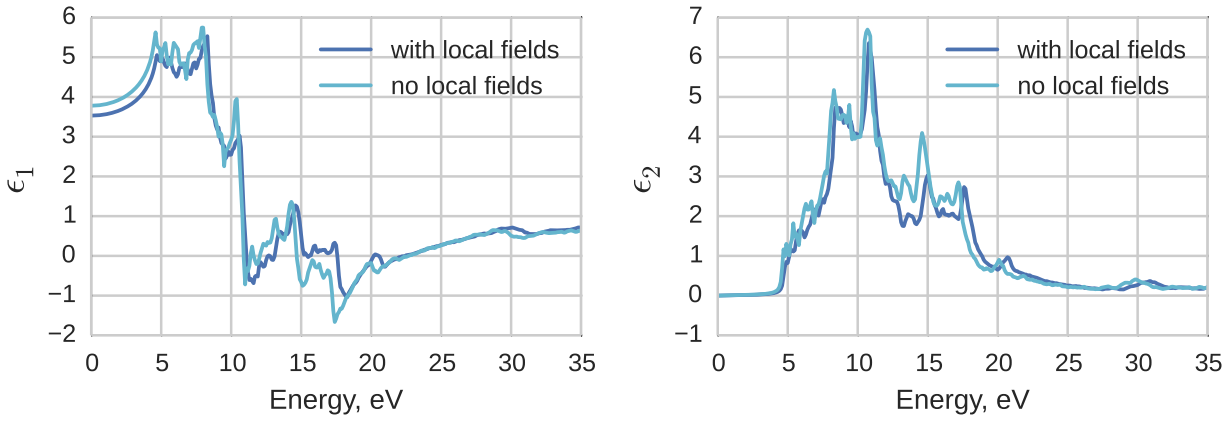

Figure 3.5: Real and imaginary part of the dielectric function calculated with RPA, without taking into account crystal local field effects (light blue) and with the local field effects (dark blue).

doesn't help either, we need to use more sophisticated approach to describe the optical properties of MgO. The excitonic effects are very important for this system and must be taken into account, as was already reported in the literature [32]. TDDFT functionals were developed recently which take into account electron-hole interaction and are able to describe even bound excitons [11, 12]; however, we choose to adopt the most advanced approach and solve Bethe-Salpeter equation, which is currently the state of the art theory for treating the electron-hole interactions.

But before we solve the Bethe-Salpeter equation, we must correct the band gap with G^0W^0. The reason for this is that the Bethe-Salpeter equation reads:

$$L = L^0 + L^0(v - W)L, \tag{3.1}$$

where $L^0 = \chi^0_{QP}$ contain the quasiparticle energies, see the BSE in transition space (2.9) where quasiparticle energies enter as ingredients. Today the most used approximation for Σ is the GW approximation (see also sections 1.6 and 1.7)

3.3 G^0W^0corrections

To find the G^0W^0corrections, we must first calculate the screening, and then calculate the self-energy (see section 2.4)). Each of the two parts requires convergence of three parameters:

1. Calculation of screening:
   - cutoff energy for the plane wave basis ⇒ basis size;
   - cutoff energy for the number of **G**-vectors ⇒ dimension of the $\epsilon_{\mathbf{GG'}}(\mathbf{q}, \omega)$ matrix;
   - number of bands to sum over.
2. Calculation of the self-energy:
   - cutoff energy for the plane wave basis ⇒ basis size;
   - cutoff energy for the number of **G**-vectors to sum over;
   - number of bands to sum over.

Both calculations of screening and self-energy require integration over the Brillouin zone, and so the results must be converged with the number of k-points. Convergence of each of the 7 parameters is interdependent, and there are no empirical recipes for the "safe" values of the parameters, because in every solid the convergence behaves differently. Moreover, the calculations are very time consuming, and scale unfavorably, which makes it impossible to "overshoot" by choosing the values which are "large enough for sure". So we face a complex problem of the multidimensional convergence, where we must consider carefully the CPU time and memory requirements. There are some things, however, that helps us greatly. First, the bandgap approaches asymptotically the converged value as the parameters are increased. Second, we know that as we increase the number of k-points, the other parameters must also increase (or at least stay the same).

Special point	G^0W^0corrections, eV
Γ	2.468
X	2.957
L	2.694

Table 3.1: G^0W^0corrections for MgO at 3 k-points.

We adopted the following strategy. First, selected small values for each of the parameters except the number of k-points, and converged each parameter while keeping the other fixed at the small grid of 256 k-points ($4 \times 4 \times 4$ Monkhorst-Pack grid, see section 2.2). Then we selected the converged values, and again converged each parameter independently. Finally, we calculated the final band gap value for this k-point grid with the obtained values.

Next, we increased the number of k-points to 864 ($6 \times 6 \times 6$ grid), and repeated the same cycle again: converged each value independently, and then calculated the bandgap with the obtained values. Here we noticed that difference that we gain by increasing the number of k-points is much greater

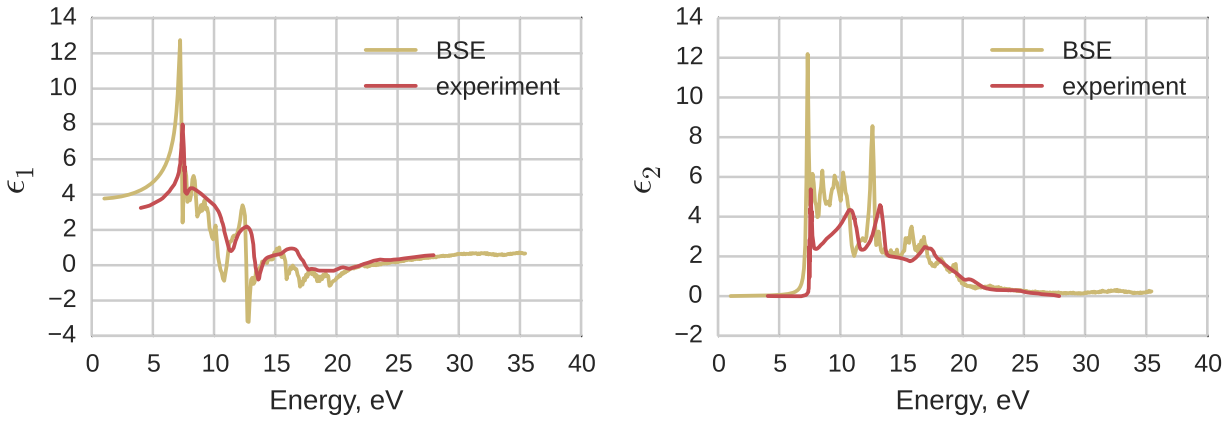

Figure 3.6: Real and imaginary part of the dielectric function calculated by solving the Bethe-Salpeter equation (BSE), compared to the experimental data [31].

than the gain from increasing the other 6 parameters. So, we move to the ($8 \times 8 \times 8$ grid). Here, the calculations become extremely time consuming, and so we quickly reach the limit of the CPU time we can afford.

The G^0W^0corrections were calculated at three k-points: Γ, X and L. The final correction values are listed in the table 3.1. As we can see, the corrections are slightly different at each of the points, suggesting that the KS DFT band dispersion can be corrected. However, for our purposes the difference, which is within 10%, can be disregarded, and we choose to correct only the band gap using the scissor operator, i.e. to widen the gap and move all the conduction bands accordingly without changing the band dispersion.

3.4 Optical and loss spectra from the Bethe-Salpeter equation

We studied excitonic properties of MgO at $\mathbf{q} = 0$ and at $\mathbf{q} > 0$ for Γ-X, Γ-L, and Γ-W directions. In the optical limit of $\mathbf{q} = 0$ we are mainly interested in the imaginary part of the dielectric function, which determines the absorption spectrum. At $\mathbf{q} > 0$ we are interested in the dynamical structure factor, which is the probability of inelastic scattering of X-rays (IXS), and in the exciton dispersion in itself.

3.4.1 Optical limit: $\mathbf{q} = 0$

The real and imaginary part of the dielectric function obtained by solving the Bethe-Salpeter equation are shown on the Figure (3.6) (the band gap of the BSE spectrum was adjusted to match the experimental value for easier comparison with experiment). The agreement between the calculated spectrum and experiment is very good. The sharp peak at the absorption edge given by the bound excitons is present, and the shape and positions of the bands in spectrum is also in good agreement.

On the Fig. 3.8a we compare the ϵ_2 with BSE and GW-RPA. The GW-RPA spectrum is a spectrum obtained with LDA wavefuntions, but with eigenvalues corrected by the scissor operator obtained from the G^0W^0calculations. There are two main qualitative differences betwen the spectra:

1. the BSE spectrum contains the sharp excitonic peak within the bandgap;
2. the oscillator strength of the BSE spectrum is red-shifted as compared to the GW-RPA spectrum.

Schematically, these differences are illustrated on the Figure 3.8b. These are the excitonic effects in the spectrum, and any method which does not take them into account fails to describe the optical properties of most of the materials, except metals.

As was described earlier (see section 2.5), there are two numerical approaches to obtain the dielectric function though the Bethe-Salpeter equation (BSE). The most straightforward way is to

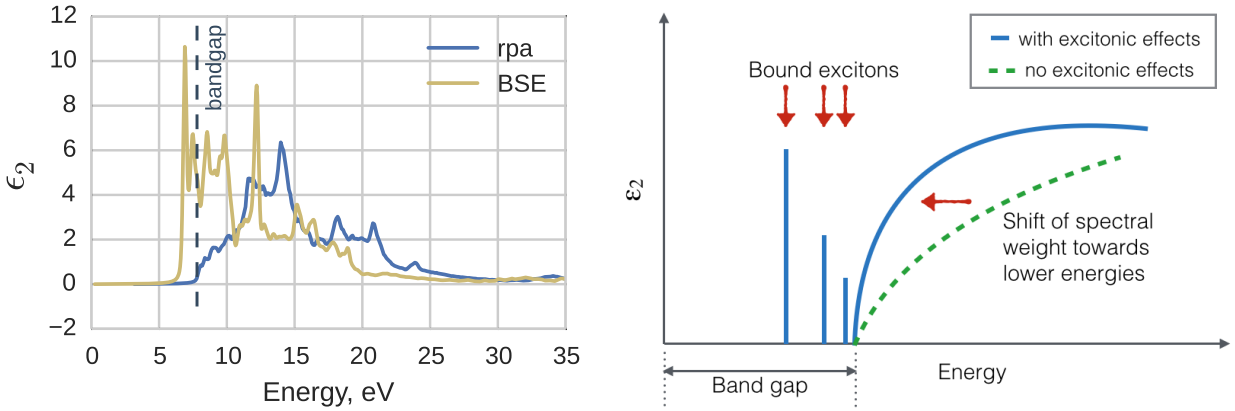

Figure 3.8: (A) Real and imaginary part of the dielectric function calculated by solving the Bethe-Salpeter equation (BSE), compared to the spectra calculated with GW RPA. (B) Schematic representation of excitonic effects in the imaginary part of dielectric function: the formation of bound excitonic peaks within the band gap, and red shift of the oscillator strength in the region of interband transitions.

diagonalize the excitonic Hamiltonian. The complexity of the algorithm is N^3, where N is the number of transitions given by the product of number of k-points, valence and conduction bands. We were able to diagonalize the Hamiltonian with 3 valence and 3 conduction bands, which yielded 18432 independent-particle transitions. With 3 conduction bands we can study only the low-energy part of the spectrum (roughly up to 9eV), however, full diagonalization yields the excitonic eigenvectors A_λ and excitonic energies E_λ, where λ is the index of excitonic states that enters the equation (2.11). Knowing them, we can not only calculate the dielectric function ϵ_M (eq. (2.11)) but also answer some important questions:

- How delocalized is the excitonic wavefunction?
- How many bound excitonic states are there? What are the binding energies of the excitons?
- Which parts of the Brillouin zone contribute to the formation of the bound excitonic states?
- How many independent-particle transitions do we need to describe the spectrum?

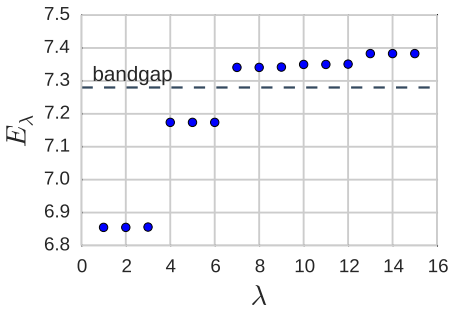

Figure 3.7: Excitonic energies E_λ for the first 15 states λ. The two triply-degenerate states below the bandgap are the bound excitonic states. The states.

Another way is to abandon the idea of the full diagonalization, and use iterative inversion algorithms, which are much faster and less memory consuming, making it possible to tackle bigger systems and include many more bands to reach higher energies. The drawback is that ϵ_M is calculated directly, without obtaining the A_λ and E_λ. So we obtain the full spectrum, but cannot analyse it as deeply as in the case of full diagonalization.

It must be noted that to converge the binding energies, one would need to use a k-point grid which contains the Γ point and is very dense in its vicinity [32]. To converge the overall spectrum, on the contrary, one needs a k-point grid which does not contain any high-symmetry points (built using the symmetry-breaking shifts, see section 2.5). As our goal was to obtain the spectra, the binding energies we obtained are not perfectly converged, even though the shape of the spectrum is correct.

The excitonic energies for the 15 lowest excitonic states λ at $\mathbf{q} = 0$ are shown at the Figure 3.7. There are two setf of triple degenerate bound excitonic states. The one with the highest binding energy is of the main importance to us. Using only 50 independent-particle transitions, the corresponding

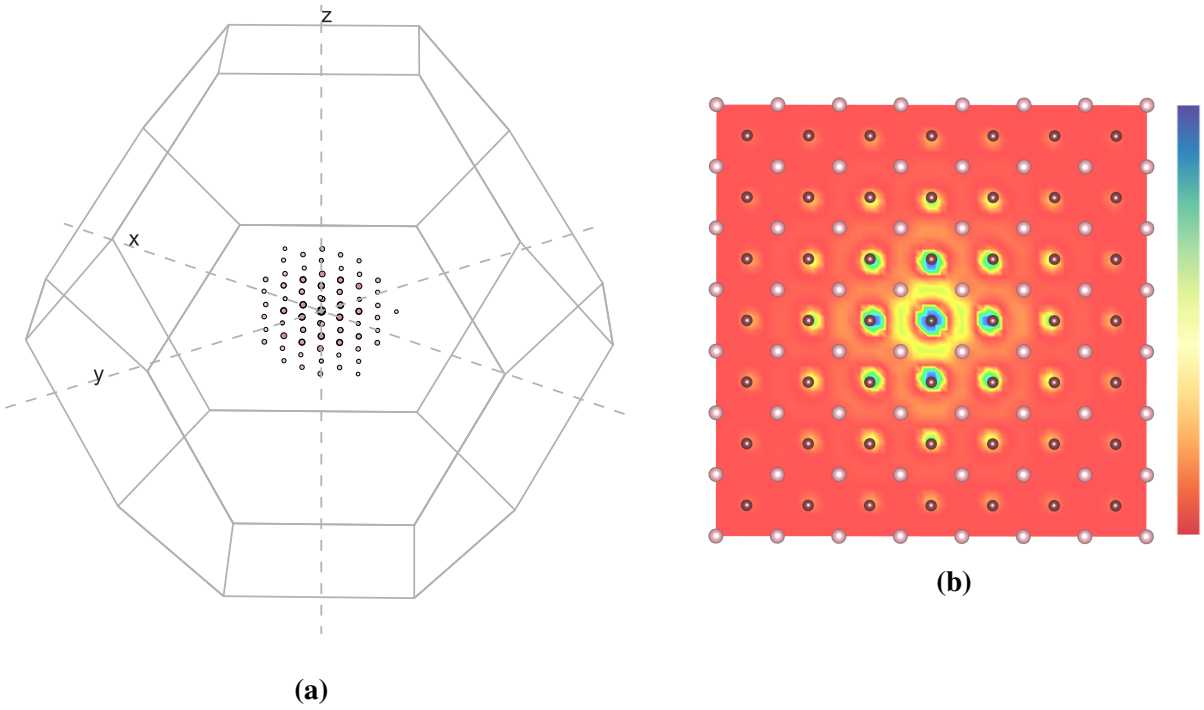

Figure 3.9: (A) Location in the Brillouin Zone of the interband transitions that form the first bound exciton. The transitions are located in the vicinity of the Γ point. (B) The lowest bound exciton: electronic density with the hole fixed on the Oxygen atom in the center (110 cut). The wavefunction is delocalized over about 5 unit cells.

peak already gains 50% of its intensity. These transitions are located in the vicinity of the Γ point, with the transition at Γ giving the greatest contribution (Fig. 3.9a).

Our analysis also shows that in order to describe features at higher energies, there's no obvious equivalent to Fig. 3.9a, for the mixing of transitions involves many more bands and spans over much larger regions of the Brillouin zone.

The excitonic wavefunction is a function of electron and hole coordinates. It cannot be represented on an image, and to visualize it, we must fix the coordinates of one of the particles. On the Figure 3.9b we show the electronic density of the lowest bound exciton with the hole fixed at the Oxygen atom in the center of the picture. The excitonic density avoids Magnesium and is concentrated on Oxygen, which confirms our expectations from the analysis of the projected density of states. The exciton is delocalized over the distance much larger than a unit cell, and in this manner it is similar to a Wannier exciton [33].

3.4.2 Dynamical structure factor and exciton dispersion: $q > 0$

It's now time to look at $\mathbf{q} > 0$, for which no reference is available in the literature. Optical analysis is not able to probe fininite $\mathbf{q}$, so we have to compare to scattering experiments, like non-resonsnt intelastic X-Ray scattering (NIXS).

The dynamical structure factor (DSF) $S(\mathbf{r}, \omega)$ describes the probability of NIXS. It is proportional to the loss function $\Im(\epsilon_M^{-1})$ (which can also be obtained from electron energy loss spectra, see eq. (1.9)):

$$S(\mathbf{r}, \omega) = -\frac{q^2}{4\pi^2 n} \Im \frac{1}{\epsilon_M} \tag{3.2}$$

where n is the average electron density. We can calculate the inverse macroscopic dielectric function directly from BSE.

On the Fig. 3.10 we show the dispersion of the exciton for small values of momentum transfer

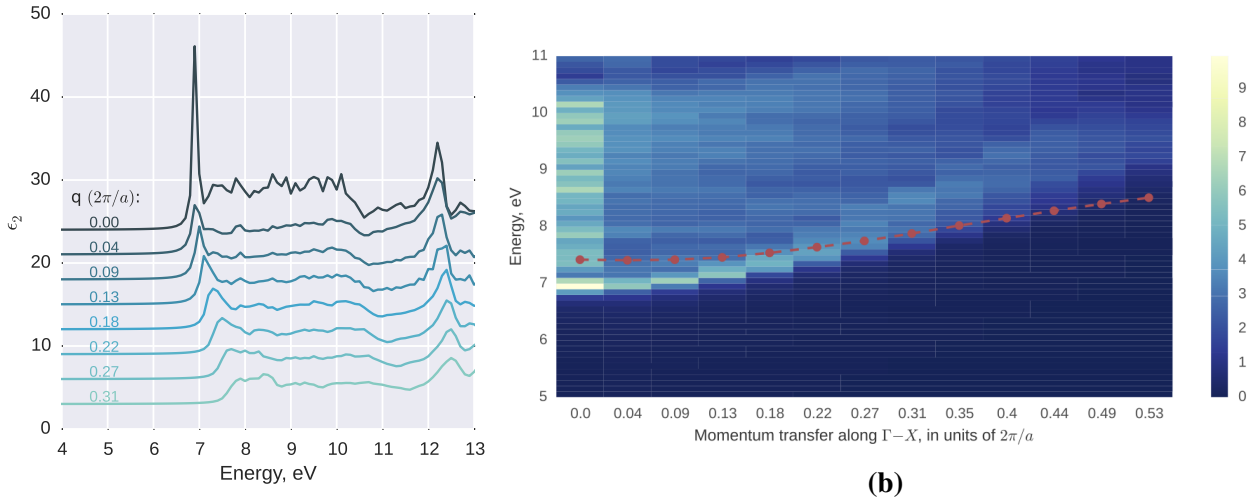

Figure 3.10: Imaginary part of the macroscopic dielectric function for the small values of momentum transfer along $\Gamma - X$ direction. Both images present the same data in the form of a pseudo-3D plot (a) and in the form of a color map (b), where the color corresponds to the intensity of the ϵ_2.

along Γ-X direction. The dispersion of the exciton is close to parabolic, which makes it similar to a Wannier model.

Clearly going away from $\mathbf{q} = 0$, the Wannier model cannot follow any longer *ab initio* calculations are necessary. and The DSF for large momentum transfer along Γ-X is shown on the Fig. 3.11. The signal from excitons in very low, and although there are bound excitonic states, they are "dark", i.e. they cannot be seen in the scattering experiment. These dark states, however, are important because they can interact with other degrees of freedom of the system and become deexcitation channels.

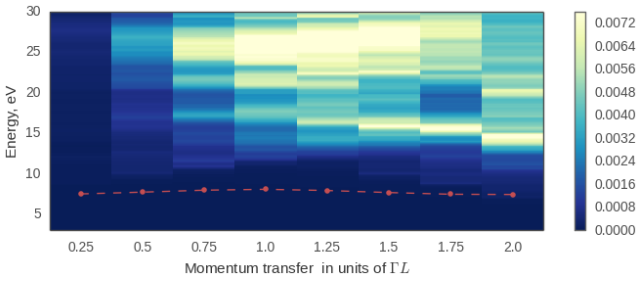

Figure 3.12: The DSF in the $\Gamma - L$ direction shows plasmonic peak, while the signal close to the bandgap (red dashed line) is virtually absent.

The exciton dispersion for the Γ-X direction is shown on the Fig. 3.11, bottom panel. Each circle corresponds to a calculated energy-momentum value. For most of the values of **q** there are three double-degenerate bound excitonic states. The degeneracy can be a consequence of the cubic symmetry, and of the degeneracy of the valence bands (see the Kohn-Sham bandstructure on the Fig. 3.2a).

The DSF for the Γ-L direction is shown on the Fig. 3.12. For this direction of momentum transfer, there is no excitonic signal whatsoever.

The DSF for less symmetric direction $\Gamma - W$ (Fig. 3.13), on the contrary, shows strong excitonic signal at certain values of the momentum transfer. On the bottom panel of the Figure 3.13 we show the DSF for $\mathbf{q} = 2\Gamma W$, $2.5\Gamma W$, and $3\Gamma W$. We can see distinct peaks within the bandgap which correspond to the bound excitonic states: one peak for $\mathbf{q} = 2\Gamma W$, $2.5\Gamma W$, and in case of $\mathbf{q} = 3\Gamma W$ there are two peaks and a band around 9 eV, which due to its proximity to the band gap is strongly affected by the electron-hole interaction.

Experiment looking for an excitonic signature in MgO should clearly start from the mentioned **q** range along Γ-W. The analysis of the excitonic signatures is still ongoing, as full diagonalization for all **q**'s is still ongoing.

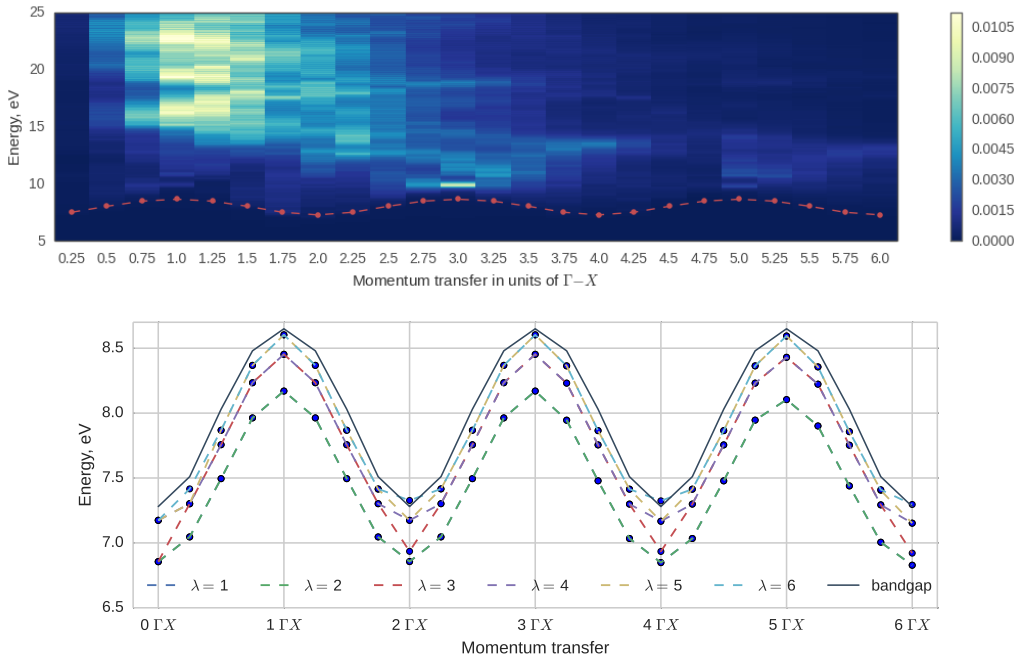

Figure 3.11: *Top:* the dynamical structure factor (DSF) for the momentum transfer **q** in the $\Gamma - X$ direction. The red dashed line is the bandgap, i.e. the lowest independent-particle transition energy for each **q**. The DSF shows strong plasmonic peak at about 20 eV, while the signal from bound excitons is too low to be visible. *Bottom:* the dispersion of the bound excitons along the $Gamma - X$ direction. Although the bound excitonic states exist, they are dark—invisible in the scattering experiment.

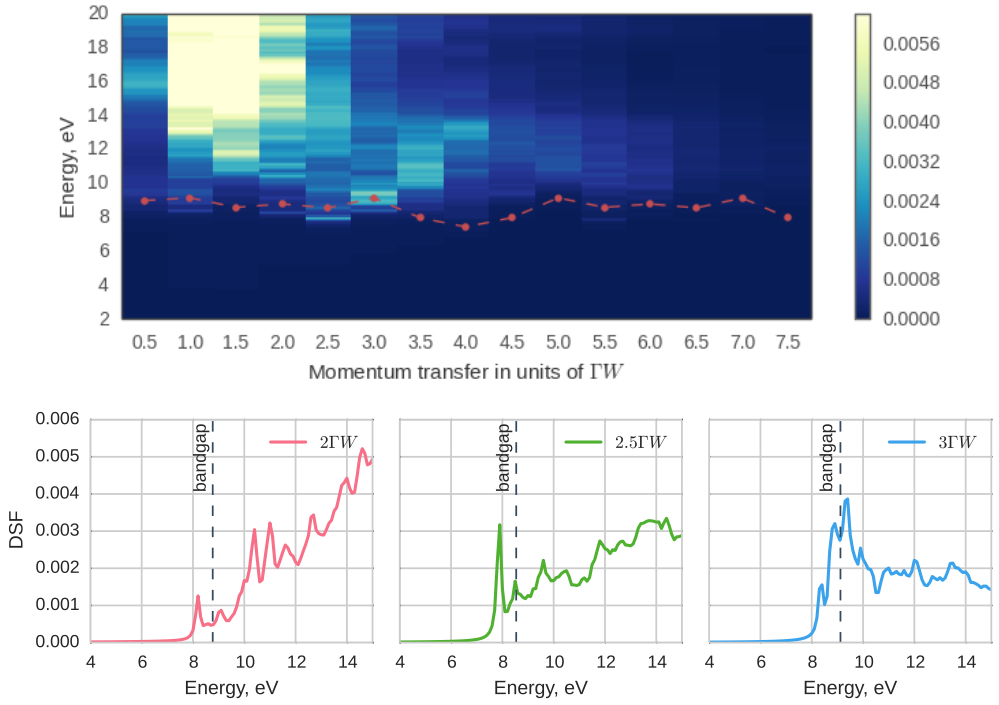

Figure 3.13: *Top:* the DSF in the $\Gamma - W$ direction shows strong plasmonic peak, as well as bound excitons and peaks close to the bandgap (red dashed line). *Bottom:* the DSF at the selected values of momentum transfer: $\mathbf{q} = 2\Gamma W, 2.5\Gamma W$, and $3\Gamma W$. The sharp peaks below the band gap correspond to the bound excitonic states.

Conclusion and Perspectives

In this thesis, we approached a problem of studying excitonic effects in MgO from the first principles in optical limit as well as at $\mathbf{q} > 0$. First, we used the formalism of time-dependent density functional theory with random phase and adiabatic local density approximations for the exchange-correlation kernel. The dielectric function obtained with both approximations drastically differs from the experiment, because they neglect excitonic effects that play an important role in dielectric properties of MgO.

Thus, we adopted a state of the art approach based on green's function formalism. We performed G^0W^0corrections for the DFT bandgap, and then obtained the dielectric function by solving the Bethe-Salpeter equation.

The resulting optical spectra show good agreement with the experiment, and reproduce the sharp excitonic peak within the bandgap, as well as the spectral features in the reegion of interband transitions. We analysed the bound exciton and determined that it is delocalized over distances much larger than a unit cell and has parabolic dispersion at small $\mathbf{q}$, which confirms that it is a Wannier-like exciton. At larger $\mathbf{q}$, however, the Wannier model breaks down, and only *ab initio* calculations are able to describe the excitonic effects.

We have calculated the dynamical structure factor at many $\mathbf{q}$'s for three directions: Γ-X, Γ-L and Γ-W, and showed that excitonic signatures are virtually absent for Γ-L, very weak for Γ-W, and strong at certain values of $\mathbf{q}$ along Γ-W. These results can be used as a suggestion for future scattering experiments, and indicate where to look for excitonic signatures.

We have validated the newly developed method of the calculation of dielectric properties at large $\mathbf{q}$ for an oxide materal. Confirmed that the method is reliable, one can study more complicated oxides, and approach the question of exciton propagation and mobility, which are important for optoelectronic applications.

There are also perspectives for theoretical description of modern synchrothron spectroscopies, e.g. coherent inelastic X-ray scattering (CIXS), resonant inelastic X-ray scattering (RIXS), which implicitly require momentum dependence and are able to study exciton and plasmon dispersion.

The dielectric function calculated with excitonic effects using Bethe-Salpeter equation can be used for more refined general theoretical description of spectroscopic experiments. For example,it can enter the theoretical description of photoemission, which will allow to describe excitonic satellites.

Bibliography

[1] Gatti, M. and Sottile, F. Oct 2013 *Phys. Rev. B* **88**, 155113.

[2] Hohenberg, P. and Kohn, W. Nov 1964 *Phys. Rev.* **136**, B864–B871.

[3] Martin, R. M. (2004) Electronic structure : basic theory and practical methods, Cambridge University Press, Cambridge, New York.

[4] Kohn, W. and Sham, L. J. Nov 1965 *Phys. Rev.* **140**, A1133–A1138.

[5] Ceperley, D. M. and Alder, B. J. Aug 1980 *Phys. Rev. Lett.* **45**, 566–569.

[6] Fetter, A. and Walecka, J. (2003) Quantum Theory of Many-particle Systems, Dover Books on PhysicsDover Publications, .

[7] Jackson, J. (1975) Classical electrodynamics, Wiley, .

[8] Marques, M., Maitra, N., Nogueira, F., Gross, E., and Rubio, A. (2012) Fundamentals of Time-Dependent Density Functional Theory, Springer, .

[9] Pines, D. (1999) Elementary Excitations in Solids: Lectures on Protons, Electrons, and Plasmons, Advanced Book Program, Perseus Books, .

[10] Kootstra, F., deBoeij, P. L., and Snijders, J. G. Sep 2000 *Phys. Rev. B* **62**, 7071–7083.

[11] Marini, A., Del Sole, R., and Rubio, A. Dec 2003 *Phys. Rev. Lett.* **91**, 256402.

[12] Reining, L., Olevano, V., Rubio, A., and Onida, G. Jan 2002 *Phys. Rev. Lett.* **88**, 066404.

[13] Gross, E., Runge, E., and Heinonen, O. (1991) Many-Particle Theory, Taylor & Francis, .

[14] Hedin, L. Aug 1965 *Phys. Rev.* **139**, A796–A823.

[15] Aryasetiawan, F. and Gunnarsson, O. (1998) *Reports on Progress in Physics* **61(3)**, 237.

[16] Guzzo, M., Lani, G., Sottile, F., Romaniello, P., Gatti, M., Kas, J. J., Rehr, J. J., Silly, M. G., Sirotti, F., and Reining, L. Oct 2011 *Phys. Rev. Lett.* **107**, 166401.

[17] vanSchilfgaarde, M., Kotani, T., and Faleev, S. Jun 2006 *Phys. Rev. Lett.* **96**, 226402.

[18] Strinati, G. (1988) *La Rivista del Nuovo Cimento* **11**, 1–86.

[19] Sasaki, S., Fujino, K., and Takeuchi, Y. (1979) *Proceedings of the Japan Academy, Series B* **55(2)**, 43–48.

[20] Bilbao crystallographic server `http://www.cryst.ehu.es`.

[21] Gonze, X., Amadon, B., Anglade, P.-M., Beuken, J.-M., Bottin, F., Boulanger, P., Bruneval, F., Caliste, D., Caracas, R., Deutsch, T., Genovese, L., Ghosez, P., Giantomassi, M., Goedecker, S., Hamann, D., Hermet, P., Jollet, F., Jomard, G., Leroux, S., Mancini, M., Mazevet, S., Oliveira, M., Onida, G., Pouillon, Y., Rangel, T., Rignanese, G.-M., Sangalli, D., Shaltaf, R., Torrent, M., Verstraete, M., Zerah, G., and Zwanziger, J. (2009) *Computer Physics Communications* **180(12)**, 2582 – 2615.

[22] Monkhorst, H. J. and Pack, J. D. Jun 1976 *Phys. Rev. B* **13**, 5188–5192.

[23] Bachelet, G. B., Hamann, D. R., and Schlüter, M. Oct 1982 *Phys. Rev. B* **26**, 4199–4228.

[24] Troullier-martins pseudopotentials `http://www.abinit.org/downloads/psp-links/psp-links/lda_tm`.

[25] Web-site of dp poject `http://www.dp-code.org/`.

[26] Benedict, L. X., Shirley, E. L., and Bohn, R. B. May 1998 *Phys. Rev. Lett.* **80**, 4514–4517.

[27] Antipov, E., Bismayer, U., Huppertz, H., Petricek, V., Pottgen, R., Schmahl, W., Tiekink, E. R. T., and Zou, X. Sep 2005 *Zeitschrift fur Kristallographie* **220**, 558?562.

[28] Godby, R. W. and Needs, R. J. Mar 1989 *Phys. Rev. Lett.* **62**, 1169–1172.

[29] Web-site of exc poject `http://etsf.polytechnique.fr/exc/`.

[30] Marsili, M. Electronic and optical properties of the (111)2x1 diamond surface: an ab-initio study. `http://etsf.polytechnique.fr/system/files/tesimarghe_dottorato.pdf` (2005).

[31] Roessler, D. M. and Walker, W. C. Jul 1967 *Phys. Rev.* **159**, 733–738.

[32] Schleife, A., Rodl, C., Fuchs, F., Furthmuller, J., and Bechstedt, F. Jul 2009 *Phys. Rev. B* **80**, 035112.

[33] Knox, R. (1963) Theory of excitons, Solid state physics: SupplementAcademic Press, .